Phosphotungstic acid/silicon carbide nanowire heterostructure photocatalyst for improving photodegradation of Rhodamine B

PENGXI LI, ZHONGHONG LIU, ZIQIZO XIA, JINGJING YANG*
Environment and Quality Test Department, Chongqing Chemical Industry Vocational College, Chongqing, 401228, P. R. China

Four different ratios of phosphotungstic acid (HPW)-silicon carbide (SiC) nanowire photocatalysts were obtained by the impregnation method, wherein HPW and SiC nanowires were the raw materials. The photocatalytic degradation performance of the synthesized photocatalysts was investigated using Rhodamine B (RhB) as the degradation substrate. The HPW/SiC nanowire composites with a 40 wt.% of HPW exhibited the best photocatalytic degradation performance; the photodegradation rate of the RhB was 82% after 240 min of irradiation, with a photodegradation rate constant of 5.07×10^{-3} min^{-1}. The results of the research conducted on the photocatalytic degradation mechanism showed that ·OH and $\cdot O_2^-$ were the main reactive species in the degradation reaction of RhB, with ·OH radicals playing a dominant role. The proposed HPW-SiC nanowire–photocatalytic material has the advantages of being low-cost, environmentally friendly, and highly efficient; additionally, it has great potential as a photocatalyst in the degradation of printing and dyeing wastewater.

(Received September 8, 2022, accepted April 7, 2023)

Keywords: Phosphotungstic acid-SiC nanowires, Photodegradation, Rhodamine B, Heterostructure

1. Introduction

Inorganic semiconductor materials powered by solar light are used for photocatalysis, which is considered a feasible strategy for dealing with the environmental pollution caused by organic chemicals [1, 2]. In the past decade, several inorganic semiconductor materials such as titanium dioxide (TiO_2) [3], tungsten trioxide (WO_3) [4], cadmium sulfide (CdS) [5], and silicon dioxide (SiO_2) [6] have been considered as effective photocatalysts for the decomposition of organic pollutants.

As a third-generation semiconductor material, silicon carbide (SiC) has attracted a lot of attention, particularly in applications such as nanowires, nanoparticles, and whiskers, owing to having outstanding properties such as a suitable bandgap (2.4-3.2 eV), a high chemical and thermal stability, a high charge-carrier mobility, and a relatively negative conduction band position for the visible light-driven photocatalytic degradation of organic pollutants [7-10]. However, it does not exhibit a satisfactory photocatalytic activity owing to its low photocatalytic degradation efficiency, high recombination rate of photoexcited e^-/h^+ pairs, and lack of active sites [11-13]. These limitations of SiC as a visible-light photocatalyst can be overcome by constructing heterojunction structures comprising two different semiconductors; examples include TiO_2/SiC [14], SnO_2/SiC [15], g-C_3N_4/SiC [16], $BiVO_4$/SiC [17], CdS/SiC [18], and graphene/SiC [19].

Phosphotungstic acid ($H_3PW_{12}O_{40}$, HPW), a typical polyoxometalate, is used in many fields, such as wastewater decontamination, acid catalysis, and desulfurization, because of its good redox properties and electronic transmission abilities [20-22]. However, it has a weak response to visible light; therefore, many studies have been devoted to the heterogenization of HPW [23-26].

SiC nanowires have a wider forbidden gap, a more positive valence-band potential, and a more negative conduction-band potential than their bulk counterparts, which results in the electron-hole pairs photogenerated using these nanowires having a stronger redox ability and these nanowires having an increased photocatalytic degradation activity [27].

In this study, we immobilized commercially available HPW on SiC nanowires using the impregnation method. We evaluated the photocatalytic activity of the synthesized photocatalysts for the degradation of Rhodamine B (RhB), which was the target organic dye, under UV irradiation; the prepared HPW/SiC nanowire composites exhibited outstanding photocatalytic activities for the degradation of RhB.

2. Experimental

2.1. Synthesis of HPW/SiC nanowire photocatalysts

Four HPW/SiC nanowire composites were synthesized using the impregnation method as follows. First, different contents of HPW, namely 10, 20, 30, 40,

and 50 wt.% of HPW, were solubilized in 25 mL of deionized water; then, 0.40 g of SiC nanowires were added. The reaction solution was mixed by stirring at room temperature for 20 h. The solution was then heated to 60 °C to support the complete evaporation of the water. The mixture was then dried at 100 °C for 8 h. Depending on the concentration of HPW, the composite photocatalytic materials were denoted as H10, H20, H30, H40, and H50.

2.2. Catalyst test

The photocatalytic activities of the HPW/SiC nanowire composites were investigated using RhB as the target pollutant. First, 0.0100 g of the photocatalytic material was added to 100 mL of RhB solution (0.01 g/L). Then, the solution was sonicated for 25 min to reach the adsorption/desorption equilibrium and irradiated with a 300 W xenon lamp (>420 nm) under continuous stirring. During irradiation, 8 mL of the reaction solution was taken at regular intervals and centrifuged for 15 min (1000 rpm). The supernatant was extracted, and the concentration of RhB was confirmed by ultraviolet-visible (UV-Vis) spectrophotometry at 554 nm.

3. Results and discussion

The X-ray diffraction (XRD) patterns of the synthesized H10, H20, H30, H40, H50, pure SiC nanowires, and HPW are shown in Fig. 1; the diffraction peaks of the immaculate SiC nanowires at 2θ=35.6° (111), 41.4° (200), 59.9° (220), and 71.7° (311) correspond to the diffraction planes of the SiC nanowires (JCPDS Card No. 75-0254). In the XRD pattern of the pure HPW, there are well-defined diffraction peaks (2θ) at 8.8, 10.8, 20.1, 26.1, 33.6, 48.5, and 61.6° corresponding to the (200), (210), (313), (423), (721), (753), and (964) planes of the HPW (ICDD Data, JCPDS Card No. 50-0655), respectively. Regarding the photocatalysts with 10 wt.% loadings (H10), no self-evident diffraction peaks were observed within the region with the 2θ<10°-separated HPW phase. The characteristic peaks became more pronounced and sharp as the content of the HPW continuously increased, from 20 to 50 wt.%. The XRD patterns of all the synthesized composites (H10, H20, H30, H40, and H50) were similar, and a characteristic peak was observed for the HPW, indicating that its Keggin structure was intact after immobilization [28].

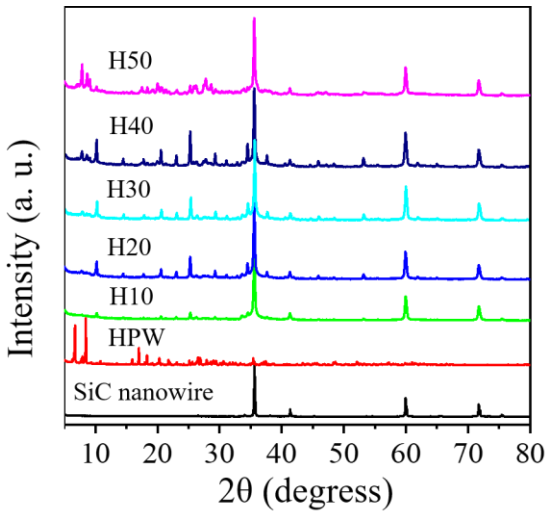

Fig. 1. X-ray diffraction (XRD) patterns of silicon carbide (SiC) nanowires, phosphotungstic acid (HPW), and serial HPW/SiC nanowire composites with different levels of HPW content (H10, H20, H40, H50) (color online)

Fig. 2 reveals the Fourier-transform infrared spectroscopy (FT-IR) spectra of the HPW, SiC nanowires, and composites (H10, H20, H30, H40, H50). Within the FT-IR spectra of the pure HPW, the peaks at 1079, 982, 892, and 805 cm^{-1} were attributed to the P-Oa asymmetric vibration, W=O bond vibration, W-Ob-W bridge bond, and W-Oc-W bridge bond, respectively [24]. Within the FT-IR spectra of the pure SiC nanowires, the characteristic absorption peak was 802 cm^{-1}, which could be attributed to the stretching vibration between C and Si [29]. However, the major absorption band of the C-Si stretching mode appeared blue-shifted after the HPW loading. Fig. 2 shows the characteristic absorption peaks of 1079 and 982 cm^{-1} that appeared for the HPW in the composite photocatalytic materials (H10, H20, H30, H40, H50); this indicated that the HPW retained its intact Keggin structure after the solid loading [22].

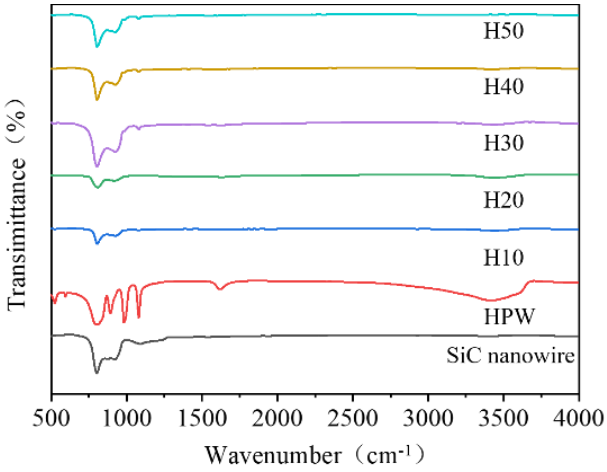

Fig. 2. Fourier-transform infrared spectroscopy (FT-IR) spectra of SiC nanowires, HPW, and serial HPW/SiC nanowire composites with different levels of HPW content (H10, H20, H40, H50) (color online)

Fig. 3 shows the UV-Vis diffuse-reflectance spectroscopy (UV-Vis DRS) spectra of different composite photocatalytic materials. The absorption wavelength of the SiC nanowires is mainly concentrated and weakened in the UV (200-400 nm) and visible regions (400-800 nm), respectively [30]. The uncovered HPW showed good light absorption properties in the UV region (200-400 nm) [24]. The significant improvement in the light harvesting ability of the HPW/SiC nanowire was attributed to the strong photo-absorption capacity of the integrated SiC nanowires. The improved UV-light absorption properties will help enhance the photocatalytic degradation activity of the HPW/SiC nanowire materials.

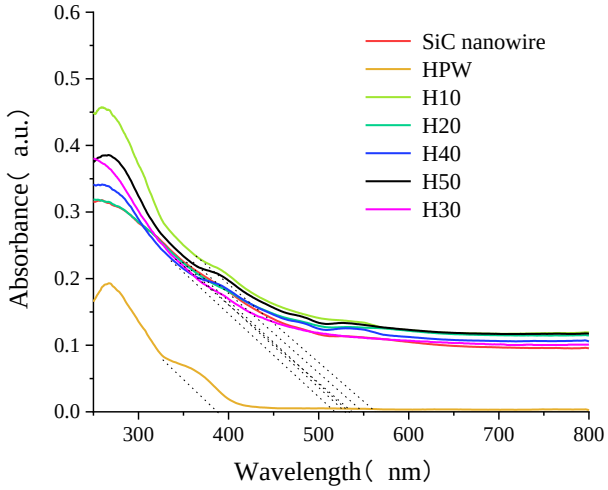

Fig. 3. UV-Vis spectra of SiC nanowires, HPW, and serial HPW/SiC nanowire composites with different levels of HPW content (H10, H20, H40, H50) (color online)

The bandgap-width of the photocatalytic materials was calculated using the formula Eg=1239.9/g, where Eg represents the band-gap width, and g represents the absorption boundary, as shown in Table 1 [31]. Compared to that of the SiC nanowire, the bandgap-widths of H10, H20, H30, and H50 were slightly lower. The bandgap-width of H40 increased to 2.40 eV, indicating that the HPW doping could change the band structure of the catalyst, improving its ability to absorb visible light and produce more electrons via photogeneration, and its overall photocatalytic efficiency.

Table 1. Bandgap of photocatalysts

photocatalytic materials	**g/nm**	**Eg/eV**
HPW	391	3.17
SiC nanowire	533	2.32
H10	558	2.22
H20	539	2.30
H30	537	2.31
H40	516	2.40
H50	549	2.25

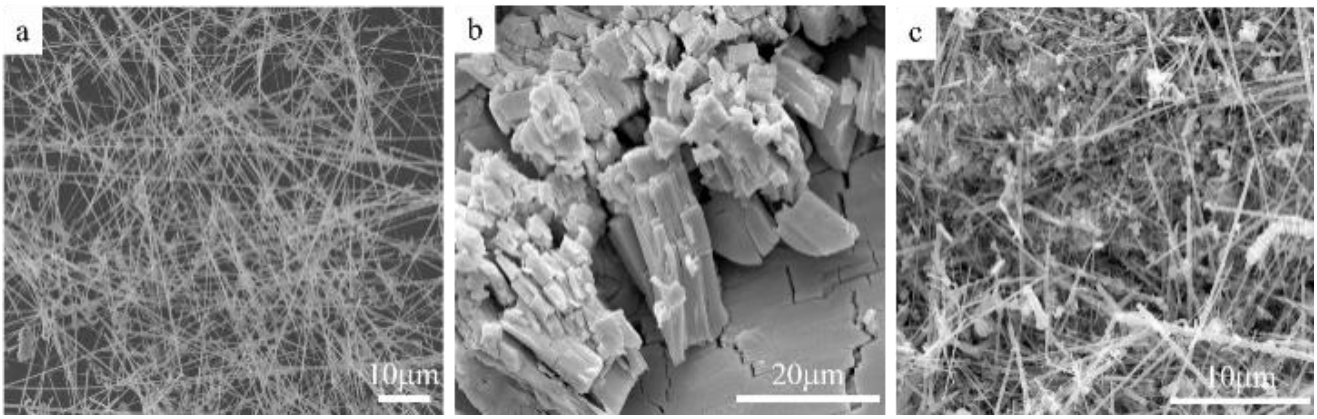

Fig. 4. Scanning electron microscopy (SEM) images of (a) SiC nanowires, (b) HPW, and (c) H10

Fig. 4 presents the scanning electron microscopy (SEM) images of the SiC nanowires, HPW and H10 while Fig. 5 presents those of a series of HPW/SiC nanowire composites with different levels of HPW (H20, H30, H40, H50). Fig. 4a shows that there are many SiC nanowires with uniform diameters of 20-200 nm and lengths in dozens of micrometers. The HPW/SiC nanowire composites resembled the SiC nanowires in shape and surface morphology (Fig. 4c, 5a-d). This indicated that the loading of the HPW in SiC nanowires did not affect the morphology of these nanowires. When the HPW loading amount was increased, the HPW species were observed as a loose stack of structures dispersed on the surface of the SiC nanowires; this arrangement was quite beneficial for the partition of the photoinduced electrons and holes.

Table 2. Comparison of degradability performances of SiC materials modified with different contents used for degrading RhB

Material	Organic Pollutant	Catalyst dosage	Concentration	Removal efficiency	References
BiOBr/SiC	RhB	0.25g/L	10mg/L	97% within 150 min	[29]
Fe_2O_3/SiC	RhB	0.1g/L	10mg/L	80% within 90 min	[30]
SiC whiskers	RhB	1.0g/L	10mg/L	52% within 6 h	[32]
SiC/$BiVO_4$	RhB	0.1g/L	10mg/L	98% within 180 min	[17]
SiC/C_3N_4	RhB	0.2g/L	10mg/L	82% within 60 min	[33]
Ag@SiC	Orange G	1.0g/L	20mg/L	65% within 240 min	[34]
B-doping SiC	methylene blue	1.0g/L	10mg/L	21.3% within 300 min	[35]

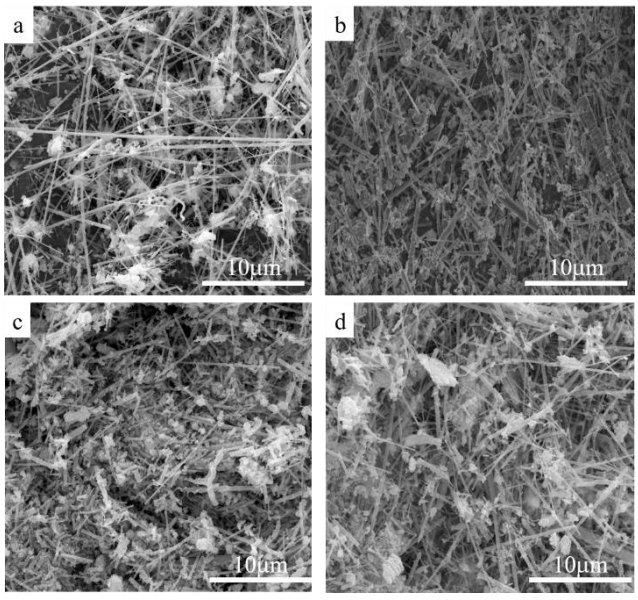

Fig. 5. SEM images of (a) H20, (b) H30, (c) H40, and (d) H50

The degradation performance of a series of HPW/SiC nanowire composites was assessed using RhB (0.01 g/L) in an aqueous solution (Fig. 6). The photodegradation efficiency of the pristine SiC nanowires was approximately 12% within 240 min. The photocatalytic activity of the HPW/SiC nanowire composites was significantly higher than that of the pure SiC nanowires. The catalytic degradation rate of H10, H20, H30, H40 and H50 were 24, 27, 71, 82, and 74%, respectively. Discernibly, the HPW/SiC nanowire composite with 40 wt.% of HPW (H40) displayed the optimal photocatalytic activity. To summarize, the results indicated that the photodegradation performance of the SiC nanowires could be improved by doping with HPW and that the photocatalytic degradation rate of the RhB solution was the highest when H40 was utilized.

The comparison of the photocatalytic activities of several SiC-based photocatalysts is shown in Table 2, these data further confirm the excellent photocatalytic performance of the HPW/SiC nanowires. Interestingly, the results of the photocatalytic degradation performance of H40 was not outstanding when compared with the results listed in Table 2. However, H40 still exhibited excellent results under demanding reaction conditions, namely a low dosage of 0.1 g/L and short reaction time of 240 min.

Table 3. Photocatalytic degradation rate constants (k) of photocatalysts used for degrading RhB

photocatalytic materials	HPW	SiC nanowire	H10	H20	H30	H40	H50
K(min^{-1}) $\times 10^{-3}$	1.69	0.47	1.30	1.09	4.43	5.07	3.73
R^2	0.944	0.868	0.789	0.718	0.987	0.992	0.989

Table 3 shows the experimental data for the photocatalytic degradation of RhB fitted with the first-order kinetic equation. The corresponding reaction rate constants for the degradation of RhB by the HPW, SiC nanowire, H10, H20, H30, H40, and H50 were 1.69×10^{-3}, 1.29×10^{-3}, 1.30×10^{-3}, 1.09×10^{-3}, 4.43×10^{-3}, 5.07×10^{-3}, and 3.73×10^{-3} min^{-1}, respectively. Among the photocatalytic materials, H40 exhibited the highest photocatalytic degradation rate. The photocatalytic degradation rate of the RhB by H40 was 11 times higher than that by the SiC nanowire, indicating the significant improvement in the photocatalytic degradation performance of the composite over that of the SiC nanowire.

The H40 catalyst was used for four cycles to degrade the RhB solution, and the stability of this catalyst was investigated (Fig. 7). H40 had strong stability, and its degradation rate was similar after four repeated stages of recycling. As the number of cycles increased, the degradation rate slightly decreased, which could be attributed to the catalyst loss during the recovery process.

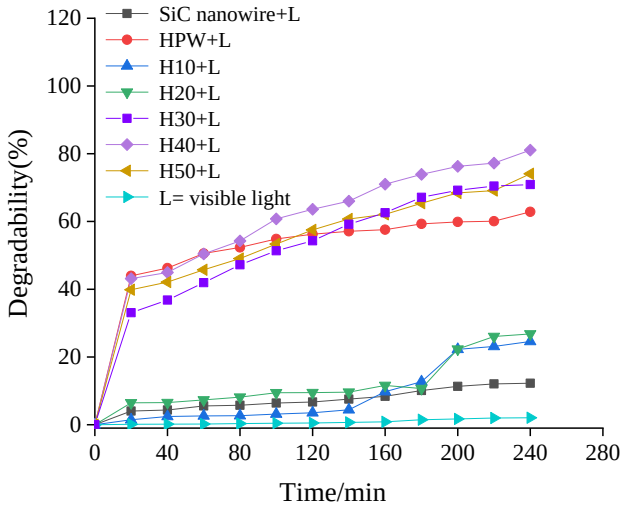

Fig. 6. Photocatalytic degradation of RhB by different composites (color online)

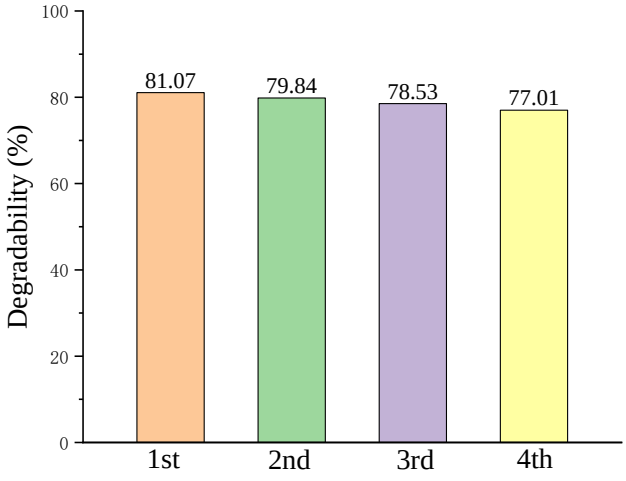

Fig. 7. Experiment wherein H40 catalyst was cyclically used to degrade RhB (color online)

The mechanism behind the photocatalytic degradation of the RhB aqeuous solution by the HPW/SiC nanowire composites was investigated by performing trapping experiments of the radical species. Isopropanol (IPA), ethylenediaminetetraacetic acid disodium salt (EDTA 2Na), and p-benzoquinone (BQ) were used to trap hydroxyl radicals (·OH), holes (h_{VB}^{+}), and superoxide radicals ($\cdot O_2^-$). A trapping agent (1 mol/ml) was added prior to irradiation with a xenon lamp for 240 min. As shown in Fig. 8, 82% of RhB has been degraded by the H40 composite under visible light irradiation in an aqueous solution without the scavenger. The degradation rate of RhB, however, dramatically decreased to 59 and 63% in the presence of the IPA and BQ, respectively, illustrating that both ·OH and O_2^- were the main reactive species in the degradation reaction of RhB, with ·OH radicals playing a dominant role. The degradation rate did not increase significantly with the addition of EDTA 2Na.

The addition of BQ resulted in a significant decrease in the degradation rate; it was concluded that the superoxide radical ($\cdot O_2^-$) was one of the main active species in the photocatalysis. After the addition of isopropyl alcohol to the reaction system, the degradation rate decreased significantly, indicating that the hydroxyl radical (·OH) was one of the main active species in photocatalysis. No significant change in the degradation rate was observed after the addition of EDTA 2Na, indicating that vacancies (h_{VB}^{+}) had played an insignificant role in photocatalytic degradation.

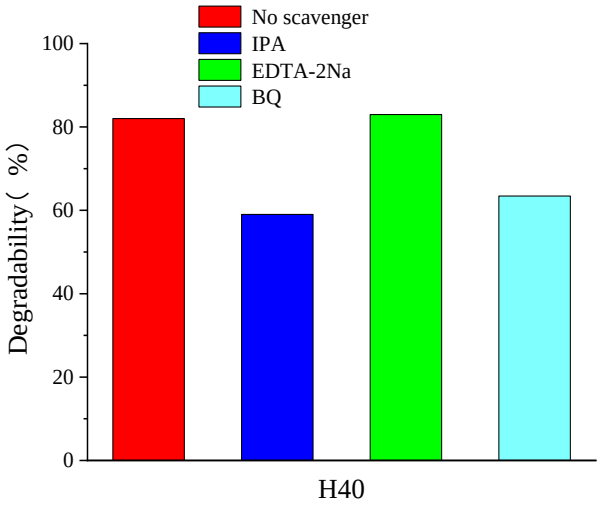

Fig. 8. Influence of different scavengers on the catalytic activity of H40 (color online)

The migration process of the photogenerated electrons over the composite catalyst is shown in Fig. 9. Since HPW has an energy band structure similar to that of metal oxide semiconductors, it acted as an effective electron trapping agent in addition to being a good photocatalytst. Additionally, it accepted the electrons generated by the photoexcitation of SiC nanowires, prolonging the photogenerated electron–hole recombination time. SiC nanowires have a conduction band and valence band of -

0.9 and +1.5 eV, respectively, while HPW has a conduction band and valence band of -0.4 and +2.6 eV, respectively [8, 25]. Since the conduction band of the SiC nanowires is more negative than that of the HPW and the valence band of the HPW is more positive than that of the SiC nanowires, the electrons migrated from the conduction band of the SiC nanowires to that of the HPW while the holes remained in the valence band of the SiC nanowires. Resultantly, the electrons and holes were effectively separated, and the probability of compounding was reduced.

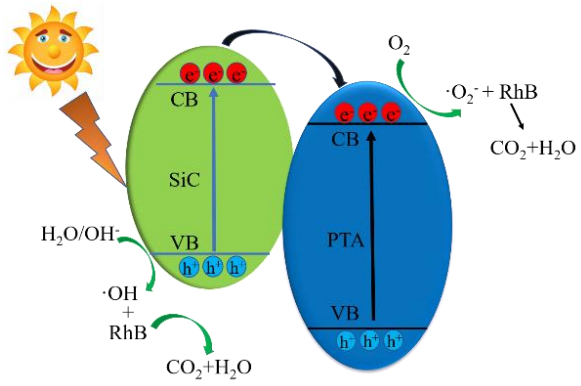

Fig. 9. Schematic illustration of degradation of RhB by HPW/SiC nanowire composite under visible light irradiation (color online)

4. Conclusions

A simple impregnation method was used to prepare a series of HPW/SiC nanowire composites. Incorporating HPW significantly affected the optical properties and photocatalytic degradation of RhB in the composites. Among them, H40 exhibited the highest photocatalytic activity, degrading 82% of the RhB within 240 min. Compared to the photocatalytic degradation rate of the RhB by the SiC nanowire, that of the RhB by H40 was 11 times higher, indicating the significant improvement in the photocatalytic degradation performance when the composite was used. The hydroxyl radical was the most active species in the photocatalytic degradation reaction, reacting with RhB and degrading it to carbon, water, and carbon dioxide, as demonstrated in the free radical capture experiments. In conclusion, the HPW/SiC nanowire composite is a promising photocatalyst for the degradation of organic dyes within wastewater.

Acknowledgements

This work was financially supported partially by the Natural Science Foundation of Chongqing, China (grant No. cstc2021jcyj-msxmX0242).

References

[1] C. C. Chen, W. Ma, J. Zhao, Chem. Soc. Rev. **39**, 4206 (2010).
[2] H. Tada, T. Kiyonaga, S. I. Naya, Chem. Soc. Rev. **38**, 1849 (2009).
[3] A. Mahmood, X. Wang, X. F. Xie, J. Sun, ACS Appl. Nano Mater. **4**, 3799 (2021).
[4] D. P. Depuccio, P. Botella, B. Rourke, C. C. Landrya, ACS Appl. Mater. Interfaces **7**, 1987 (2015).
[5] K. Azam, Z. Rehman, R. Muneebur, R. Khan, Zulfiqar, A. Waseem, A. Iqbal, Z. H. Shah, Inorg. Chem. Commun. **72**, 33 (2016).
[6] A. Cd, A. Ji, Y. B. Zhe, Y. Xiao, M. Xing, J. Zhang, Chinese Chem. Lett. **30**, 853 (2019).
[7] J. H. Eom, Y. W. Kim, S. Raju, J. Asian Ceram. Soc. **1**, 220 (2013).
[8] J. Zhang, J. Chen, L. Xin, M. Wang, Mat. Sci. Eng. B **179**, 6 (2014).
[9] N. D. Shcherban, J. Ind. Eng. Chem. **50**, 15 (2017).
[10] R. Wu, K. Zhou, C. Y. Yue, J. Wei, Y. Pan, Prog. Mater. Sci. **72**, 1 (2015).
[11] J. Hong, S. M. Seyyed, B. Vitaliy, C. Huang, S. Luanwuthi, J. Acapulco, P. Holdway, P. S. Grant, N. Grobert, Appl. Catal. B **218**, 267 (2017).
[12] M. M. Wang, J. Chen, X. Liao, Z. Liu, J. Zhang, L. Gao, Y. Li, Int. J. Hydrogen Energ. **39**, 14581 (2014).
[13] J. Y. Hao, Y. Y. Wang, X. L. Tong, G. Jin, X. Guo, Int. J. Hydrogen Energ. **37**, 15038 (2012).
[14] M. Gopa, K. M. Parida, S. K. Singh, ACS Sustainable Chem. Eng. **3**, 245 (2015).
[15] X. Liao, J. Chen, M. Wang, Z. Liu, L. Ding, Y. Li, J. Alloy. Compd. **658**, 642 (2016).
[16] H. Zhu, B. Yang, J. Yang, Y. Yuan, J. Zhang, Chemosphere **276**, 130217 (2021).
[17] J. Yang, Y. Peng, B. Yang, J. Disper. Sci. Technol. **40**, 408 (2019).
[18] Y. Peng, Z. N. Guo, J. J. Yang, D. Wang, W. Yuan, J. Mater. Chem. A **2**, 6296 (2014).
[19] H. Kohno, Y. Kazuki, N. Hirohiko, Jpn. J. Appl. Phys. **50**, 18001 (2011).
[20] S. Omwoma, Gore C. T., Y. Ji, C. Hu, Song, Y. Fei, Coordin. Chem. Rev. **286**, 17 (2015).
[21] A. Olgun, A. T. Çolak, H. Gübbük, O. Şahin, E. Kanar, J. Mol. Struct. **1134**, 78 (2017).
[22] X. J. Sun, J. Zhang, Z. Y. Fu, ACS Appl. Mater. Interfaces **10**, 35671 (2018).
[23] Q. Wang, D. Jiao, Y. Bai, J. Zhong, L. Zhao, X. Yong, J. Tong, J. Li, Mater. Lett. **161**, 267 (2015).
[24] E. P. Ferreira, S. Ullah, F. L. Carvalho, A. L. Souza, M. Oliveira, J. F. Schneider, Y. P. Mascarenhas, A. M. Jorge, U. P. Rodrigues, Mater. Chem. Phys. **153**, 410 (2015).
[25] P. Meng, H. Heng, Y. Sun, J. Huang, J. Yang, L. Xia, Appl. Catal. B **226**, 487 (2018).
[26] X. You, L. Yu, F. Xiao, S. Wu, C. Yang, J. Cheng, Chem. Eng. J. **335**, 335 (2017).
[27] J. Zhang, J. Chen, L. Xin, M. Wang, Mat. Sci. Eng. B **179**, 6 (2014).
[28] B. C. Ong, H. K. Lim, C. Y. Tay, T. Lim, Z. Dong,

Chemosphere **286**, 131869 (2022).
[29] Z. H. Hou, J. P. Chen, L. J. Xie, X. X. Wei, C. M. Chen, Appl. Surf. Sci. **543**, 148779 (2021).
[30] Y. Peng, X. Guo, J. Yang, T. Xie, J. Wang, S. Liu, J. Disper Sci. Technol. **43**, 629 (2020).
[31] J. Jiang, Z. Xiong, H. Wang, G. Liao, S. Bai, J. Zou, P. Wu, P. Zhang, X. Li, J. Mater. Sci. Technol. **118**, 15 (2022).
[32] J. Chen, G. Song, Z. Liu, Q. Kong, S. Zhang, C. Chen, J. Alloy. Compd. **833**, 155072 (2020).
[33] J. Yang, Y. Peng, B. Yang, P. Li, Mater. Res. Express **5**, 85511 (2018).
[34] S. Adhikari, N. K. Eswar, S. Sangita, D. Sarkar, G. Madras, J. Photoch. Photobio. A **357**, 118 (2018).
[35] N. Koysuren, Polym-Plast. Tech. Mat. **60**, 1620 (2021).

*Corresponding author: hahajing1229@163.com